Anomalous Long-Distance Coherence in Critically Driven Cavity Magnonics

Ying Yang [●],[1] Jiguang Yao [●],[1] Yang Xiao [●],[2] Pak-Tik Fong [●],[3] Hoi-Kwan Lau [●],[3,4] and C.-M. Hu [●][1,*]

[1]*Department of Physics and Astronomy, University of Manitoba, Winnipeg R3T 2N2, Canada*
[2]*Department of Physics, Nanjing University of Aeronautics and Astronautics, Nanjing 210016, China*
[3]*Department of Physics, Simon Fraser University, Burnaby V5A 1S6, Canada*
[4]*Quantum Algorithms Institute, Surrey, British Columbia V3T 5X3, Canada*

Developing quantum networks necessitates coherently connecting distant systems via remote strong coupling. Here, we demonstrate long-distance coherence in cavity magnonics operating in the linear regime. By locally setting the cavity near critical coupling with traveling photons, nonlocal magnon-photon coherence is established via strong coupling over a 2-m distance. We observe two anomalies in this long-distance coherence: first, the coupling strength oscillates twice the period of conventional photon-mediated couplings; second, clear mode splitting is observed within the cavity linewidth. Both effects cannot be explained by conventional coupled-mode theory, which reveals the tip of an iceberg of photon-mediated coupling in systems under critical driving. Our Letter shows the potential of using critical phenomena for harnessing long-distance coherence in distributed systems.

Introduction.—Coherent dynamics enabled by strong light-matter interactions [1–3] contributes significantly to the advancements in quantum science and technology, which are typically achieved by overlapping electromagnetic fields. When systems are separated by macroscopic distances, the direct coupling is hindered due to the reduced overlap of fields, posing a challenge for establishing and preserving long-distance coherence.

To achieve long-distance coherence, several methods are employed, such as optomechanical systems [4], superconducting cavities [5], topological edge states [6], and surface acoustic waves [7]. One of the most interesting methods involves traveling photons in microwave waveguides, laser beams, or optical fibers [8–11]. Indirect couplings between distant resonators are generated through their cooperation of dissipations to traveling photons [12,13], which has garnered broad interest in quantum optics [14,15] and waveguide quantum electrodynamics [16–18].
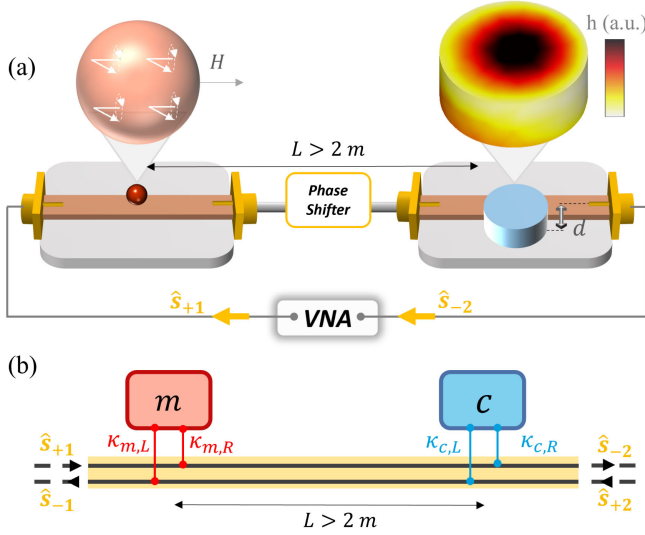
The main difficulty for implementing this approach is dissipation: in conventional systems where a pair of resonators are connected by traveling photons, the same photons that mediate the coupling induce an extrinsic dissipation, causing photon-induced decoherence that erases the photon-mediated coherence [19–22]. In order to establish long-distance coherence, special methods are employed for either enhancing the coupling or suppressing the dissipation. For example, long-distance strong coupling has been demonstrated by terminating the waveguide with mirrors [17,23–25], adopting a light loop [22,26], constructing resonators as giant atoms [27–29], or utilizing a gain-driven cavity [30,31]. While these methods enhance the cooperativity, they also come with drawbacks such as

bandwidth limitations, stability constraints, design challenges, and nonlinear disruptions.

Recently, cavity magnonics [2] has emerged as a versatile platform for engineering light-matter interactions. Among many advantages, it enables the incorporation of critical phenomena, such as exceptional points and bound states in the continuum in coupled systems. Experiments have found that by using critical phenomena, dissipations can be harnessed as a resource [32]. This sparks curiosity about whether cavity magnonics could pave the way for establishing coherence over long distances by utilizing critical phenomena.

This Letter experimentally explores such a frontier by studying critically driven cavity magnonics. A cylindrical dielectric cavity [33] is used to study its remote coupling with an yttrium iron garnet (YIG) sphere [34]. The coupling is mediated by photons traveling in coaxial cables over 2 m long. Near the critical-driving condition where the cavity is critically coupled to traveling photons, we observe a normal mode splitting that demonstrates coherent energy exchange mediated by photons traveling over a long distance. Moreover, by comparing with standard theories for photon-mediated coupling, we show that the observed coupling is anomalous in both the coupling strength and its dependence on the phase of the traveling photons.
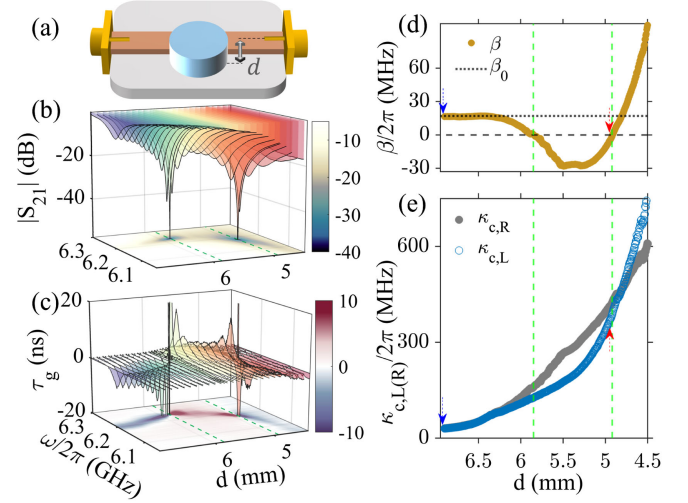
Setup.—Our setup is shown in Fig. 1(a). The YIG sphere with 1 mm diameter is placed on a 4.65 mm-wide microstrip. It is biased by an external magnetic field H applied parallel to the microstrip, which controls the resonant frequency $\omega_m = \gamma_e \mu_0 (H + H_A)$ of the magnon mode. Here, μ_0 is the vacuum permeability. From calibrations [35], we get the gyromagnetic ratio $\gamma_e = 2\pi \times 22.4$ GHz/T, the anisotropy

FIG. 1. Setup. (a) The YIG sphere is placed on a microstrip. An external magnetic field H applied parallel to the microstrip drives the magnon mode with the uniform precession. The dielectric cylinder is placed on another microstrip. The cavity mode profile in the top right resembles the TE01 mode. The lateral spacing d between the centers of the cavity and the microstrip is tunable by using a step motor. The magnon and cavity modes are coupled remotely via photons traveling in coaxial cables that connect the microstrips. The traveling phase $\Phi = \Phi_L + \Delta\Phi$ is controlled by an inserted phase shifter that tunes $\Delta\Phi$, while $\Phi_L = 2\pi L/\lambda$ is set by the photon propagation distance L. The transmission spectra $S_{21}(\omega)$ are measured by connecting the end ports of the microstrips to the vector network analyzer. (b) Theoretical model. The magnon and cavity photon modes are coupled to the traveling photons with rates $\kappa_{m,L(R)}$ and $\kappa_{c,L(R)}$, respectively, and measured by input $\hat{s}_{+1}$ and output $\hat{s}_{-2}$ fields.

FIG. 2. Critical coupling. (a) The dielectric cylinder is calibrated by tuning its lateral spacing d to the microstrip. (b) The transmission amplitude $|S_{21}|$ and (c) group delay τ_g reveal two critical coupling conditions marked by the green dashed lines. (d) The effective damping rate $\beta/2\pi$ and (e) the extrinsic damping rate $\kappa_{c,L(R)}/2\pi$ are extracted by fitting the transmission using Eq. (1). The dotted line in (d) shows the intrinsic damping rate $\beta_0/2\pi$. The arrows in (d) and (e) mark the cavity setting conditions for the data presented in Figs. 3 and 4.

field $\mu_0 H_A = -7.1$ mT, the intrinsic magnon damping rate $\alpha_0/2\pi = 0.8$ MHz, and the rates of extrinsic damping of the magnon mode to the left-going ($\kappa_{m,L}/2\pi = 8$ MHz) and right-going ($\kappa_{m,R}/2\pi = 7$ MHz) traveling waves [schematically shown in Fig. 1(b)].

A dielectric cylinder [33], with a diameter of 9.1 mm, a height of 3.7 mm and a dielectric constant of 34, is placed on another 4.65 mm-wide microstrip. In the top right of Fig. 1, the simulated cavity mode profile is plotted, resembling the TE01 mode where a magnetic dipole is along the vertical axis of the cylinder. The lateral spacing d between the centers of the cavity and the microstrip is tunable by a step motor. The two microstrips are connected by coaxial cables with a total length L, and a phase shifter is inserted into the cables.

Our goal is to establish nonlocal coherence between the magnon and cavity modes via photons traveling in the coaxial cables. At $\omega/2\pi = 6.2$ GHz (wavelength $\lambda = 32.7$ mm), the traveling phase between the magnon and photon modes is $\Phi = \Phi_L + \Delta\Phi$, where $\Phi_L = 2\pi L/\lambda > 128\pi$ is the phase of the photons propagating over a distance of $L > 2$ m [35]. $\Delta\Phi$ is controlled by the phase shifter,

precisely tuning Φ over a period of 2π. The transmission spectra $S_{21}(\omega)$ are measured by connecting the end ports of the microstrips to the vector network analyzer. The experiments are performed in the linear dynamics regime by setting the input power at -10 dBm.

Critical coupling.—We calibrate the critical coupling [52] between the cavity and microstrip to construct critically driven cavity magnonics. The condition is set by the lateral spacing d that controls cavity-microstrip coupling. In the calibration measurement, the YIG sphere is unbiased by setting $H = 0$, and the phase shifter is set at $\Delta\Phi = \pi$.

Figures 2(b) and 2(c) plot the measured transmission amplitude $|S_{21}(\omega)|$ and the group delay $\tau_g(\omega) = -\partial\angle S_{21}/\partial\omega$ of the cavity, respectively, where $\angle S_{21}$ is the transmission phase. By changing d, the cavity mode frequency ω_c shifts nonmonotonically. Two sharp dips are observed at $d = 4.90$ and 5.80 mm in Fig. 2(b), each marked by a green dashed line. These are the critical coupling conditions, as we explain below. At these conditions, $|S_{21}(\omega_c)|$ approaches zero in the linear scale, while $\tau_g(\omega_c)$ switches abruptly between positive and negative infinities. In the region between the two dashed lines, $\tau_g(\omega_c) > 0$; outside of the region, $\tau_g(\omega_c) < 0$.

Using the input-output theory [53,54], we derive [35]

$$S_{21} = \frac{\omega - \omega_c + i(\beta_0 + \kappa_{c,L}/2 - \kappa_{c,R}/2)}{\omega - \omega_c + i(\beta_0 + \kappa_{c,L}/2 + \kappa_{c,R}/2)}, \quad (1)$$

where the intrinsic damping rate of the cavity mode is calibrated as $\beta_0/2\pi = 17$ MHz. $\kappa_{c,L}/2\pi$ and $\kappa_{c,R}/2\pi$ are the rates of extrinsic damping of the cavity mode to the left-going and right-going traveling waves, respectively. Both of them depend on d.

Equation (1) shows that $1/|S_{21}(\omega)|$ has a Lorentzian line shape with HWHM $= |\beta|$, where β is an effective damping rate defined as

$$\beta = \beta_0 + \kappa_{c,L}/2 - \kappa_{c,R}/2. \tag{2}$$

It models the cavity as a loaded oscillator with $\tilde{\omega}_c = \omega_c - i\beta$, where the loading effect of the traveling photons impacts both HWHM and τ_g. At the resonance, $\tau_g(\omega_c) \propto -(1/\beta)$, so that β determines the sign of $\tau_g(\omega_c)$: when $\beta > 0$, we have $\tau_g(\omega_c) < 0$, the cavity is undercoupled to the traveling photons; when $\beta < 0$, the cavity is over-coupled, leading to $\tau_g(\omega_c) > 0$; at $\beta = 0$, the cavity is critically coupled, which is a singularity where $\tau_g(\omega_c)$ approaches infinity [52].

Using Eq. (1) to fit the measured S_{21} spectra [35], we deduce the fitting parameters $\kappa_{c,L}$ and $\kappa_{c,R}$ and plot them in Fig. 2(e). β is determined from Eq. (2) and plotted in Fig. 2(d). Note that due to an interference effect [27,28,55–59], when d decreases, $\kappa_{c,L}$ and $\kappa_{c,R}$ increase differently with the enhanced field overlapping of the cavity and microstrip, so that β oscillates, which leads to two critical coupling conditions at $d = 4.90$ and 5.80 mm [35]. Near both critical conditions, the cavity mode dynamically functions as a loaded high-Q oscillator with nearly zero effective damping, which is extremely sensitive to detect long-distance coherence, as we demonstrate below in two experiments.

Photon-mediated long-distance coupling.—The first experiment, performed at different Φ while setting the H field at $\omega_m = \omega_c$, searches for the evidence of mode splitting caused by photon-mediated coupling. Typical results are comparatively presented for $d = 4.92$ mm [marked by the red arrow in Fig. 2(d)] and $d = 6.90$ mm (blue arrow). Table I lists the cavity parameters at these settings.

At $d = 4.92$ mm, three key features are observed. (i) Mode splitting is found in $|S_{21}|$ plotted in Fig. 3(a), which depends on the phase $\Phi = \Phi_L + \Delta\Phi$ (without loss of generality, we denote $\Delta\Phi = \pi$ at the maximum mode

splitting). This feature demonstrates that the magnon and cavity photon modes are coupled remotely by the traveling photons. Such a nonlocal hybridization leads to two normal modes $\tilde{\omega}_\pm = \omega_\pm - i\delta_\pm$, where $\omega_\pm$ and $\delta_\pm$ are the resonant frequencies and damping rates, respectively. (ii) The measured group delay of the hybridized modes exhibits antisymmetric phase dependence as shown in Fig. 3(b). For $\Delta\Phi < \pi$, we observe $\tau_g > 0$ for the higher-frequency mode $\tilde{\omega}_+$, and $\tau_g < 0$ for $\tilde{\omega}_-$; when $\Delta\Phi > \pi$, the results are reversed. This feature is associated with the anomalous phase period that we will show below. (iii) For both modes, τ_g switches abruptly between positive and negative infinities at $\Delta\Phi \simeq \pi$, where the nonlocally hybridized modes are critically coupled with the traveling photons.

As the first step for understanding these intriguing features, we model the nonlocal hybridization as two harmonic oscillators ($\tilde{\omega}_m = \omega_m - i\alpha$ and $\tilde{\omega}_c = \omega_c - i\beta$) coupled by a complex rate G. Here, $\alpha \equiv \alpha_0 + \kappa_{m,L}/2 - \kappa_{m,R}/2 = 1.3$ MHz is the effective damping rate for the
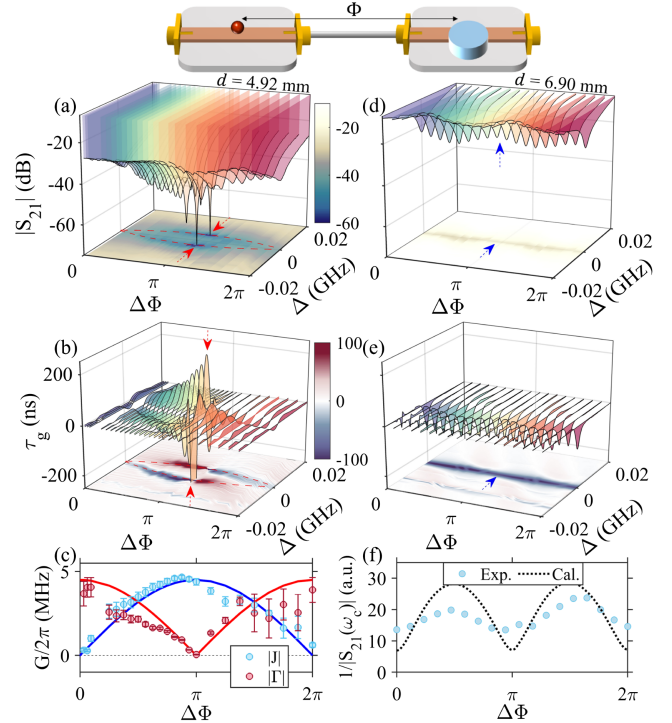

FIG. 3. Long-distance coupling: the phase dependency. The left and right panels compare the results measured at $d = 4.92$ and 6.90 mm, respectively. (a),(d) Transmission amplitude $|S_{21}|$; (b), (e) group delay τ_g measured as a function of the frequency detuning $\Delta = (\omega - \omega_c)/2\pi$ at different phase setting $\Delta\Phi$. The dashed curves in (a) and (b) are calculated by using Eq. (5) with $\eta = 2$ and $\delta = 0.996$. (c) The real and imaginary components of the complex coupling strength $G = J + i\Gamma$ are plotted as blue and red circles, while the solid sinusoidal curves are added to guide the eye. (f) The measured inverse amplitude $1/|S_{21}(\omega_c)|$ are plotted in comparison with the result calculated using Eq. (5) with $\eta = 1$ and $\delta = 1$.

TABLE I. Cavity parameters at typical settings near or away from the critical coupling (c.c), calibrated at $\Delta\Phi = \pi$.

Cavity setting	Near c.c.	Away from c.c.
d (mm)	4.92	6.90
$\omega_c/2\pi$ (GHz)	6.181	6.203
$\kappa_{c,L}/2\pi$ (MHz)	332.4	37.0
$\kappa_{c,R}/2\pi$ (MHz)	370.0	37.0
$\beta/2\pi$ (MHz)	−1.8	17.0

magnon mode. Fitting $1/|S_{21}|$ with the line shapes involving two resonances, we determine $\tilde{\omega}_{\pm} = \omega_{\pm} - i\delta_{\pm}$, from which we extract [35]

$$G = J + i\Gamma = \sqrt{(\tilde{\omega}_+ - \tilde{\omega}_-)^2 - (\tilde{\omega}_c - \tilde{\omega}_m)^2}. \quad (3)$$

Figure 3(c) plots the phase dependence of the real ($|J|$) and imaginary ($|\Gamma|$) components of G. Both J and Γ follow a sinusoidal solid curve, and G changes from purely real (coherent coupling) to purely imaginary values (dissipative coupling) when Φ changes π. This is surprising, since conventional photon-mediated coupling theory predicts that $G \sim e^{i\Phi}$, changing from purely real to purely imaginary values when Φ changes $\pi/2$ [60,61]. The anomalous doubled phase period is also observed by setting the cavity near the second critical coupling condition at $d = 5.87$ mm [35].

In contrast, at $d = 6.90$ mm, the result is different, as shown in Figs. 3(d)–3(f). Here, no mode splitting is found. Instead, a single resonance with a negative group delay τ_g is observed. A noteworthy feature is that $1/|S_{21}(\omega_c)|$ shows a phase-dependent oscillation, which we will analyze later by using the coupled-mode theory.

To confirm these typical features, we perform the second experiment at different field detuning $\Delta_m = [\omega_m(H) - \omega_c]/2\pi$, while fixing $\Delta\Phi = \pi$. Here, we compare the field dispersions measured at $d = 4.92$ and 6.90 mm.

At $d = 4.92$ mm, the measured dispersion plotted in Fig. 4(a) reveals level repulsion between the remote magnon and cavity modes, and the spectra plotted in Fig. 4(b) show anticrossing with amplitude exchange. This demonstrates coherent energy exchange between the two remote modes. From the splitting measured at $\Delta_m = 0$, we determine the coupling rate $|G| = 4.18$ MHz, corresponding to a cooperativity $C = |G|^2/|\beta\alpha| = 7.5$, which confirms that the critically driven cavity magnonics operates in the strong-coupling regime [2]. In contrast, at $d = 6.90$ mm, neither level repulsion nor anticrossing are observed. The magnon mode appears to be superimposed on the broad background of the cavity mode.

Thus, two sets of experiments consistently reach the same conclusion: by setting the cavity near the critical coupling condition, long-distance coherence is established between the remote magnon and photon modes, revealing an anomalous long-distance strong coupling mediated by traveling photons.

Phenomenological model.—Exploring beyond the simple model of Eq. (3), we now quantitatively analyze the data using the coupled-mode theory [19]. As depicted in Fig. 1(b), the magnon ($\hat{m}$) and cavity ($\hat{c}$) modes, with intrinsic damping rates $\alpha_0/2\pi$ and $\beta_0/2\pi$, respectively, are coupled to the traveling photons with rates $\kappa_{m,L(R)}/2\pi$ and $\kappa_{c,L(R)}/2\pi$, respectively. The remotely coupled system is
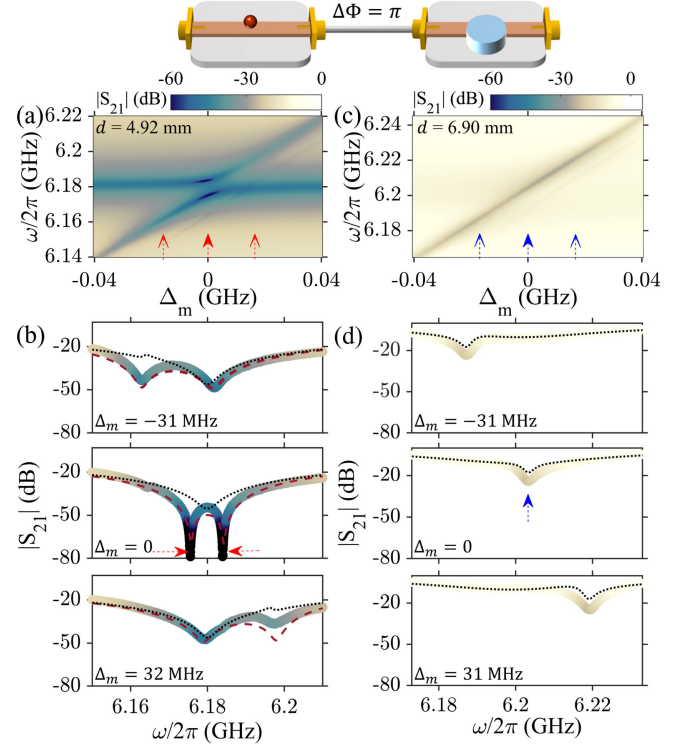

FIG. 4. Long-distance coupling: the field dependency. The left and the right panels compare the results measured at $d = 4.92$ and 6.90 mm, respectively. (a),(c) $|S_{21}|$ mapping plotted as a function of the probing frequency ω and the field detuning Δ_m, showing level repulsion caused by remote coupling. (b),(d) Transmission spectra plotted with the same color bar as in the top panel. Hybridized modes are indicated in (b) by the red arrows at $\Delta_m = 0$. The black dotted curves and the red dashed curves are theoretical calculations using Eq. (5) with $\eta = 1, \delta = 1$ and $\eta = 2, \delta = 0.996$, respectively.

driven by the input field $\hat{s}_{+1}$ and probed by the output field $\hat{s}_{-2}$. The coupled equations for $\hat{c}$ and $\hat{m}$ are

$$\begin{pmatrix} \dot{\hat{c}} \\ \dot{\hat{m}} \end{pmatrix} = -i \begin{pmatrix} \omega_c - i\beta_0 - i\kappa_c & -ie^{i\Phi/\eta}\sqrt{\kappa_{c,R}\kappa_{m,R}} \\ -ie^{i\Phi/\eta}\sqrt{\kappa_{c,L}\kappa_{m,L}} & \omega_m - i\alpha_0 - i\kappa_m \end{pmatrix} \begin{pmatrix} \hat{c} \\ \hat{m} \end{pmatrix}$$
$$- i \begin{pmatrix} e^{i\Phi/\eta}\sqrt{\kappa_{c,R}} \\ \delta\sqrt{\kappa_{m,R}} \end{pmatrix} \hat{s}_{+1},$$

$$\hat{s}_{-2} = \hat{s}_{+1} - i \begin{pmatrix} e^{-i\Phi/\eta}\sqrt{\kappa_{c,R}} & \delta\sqrt{\kappa_{m,R}} \end{pmatrix} \begin{pmatrix} \hat{c} \\ \hat{m} \end{pmatrix}, \quad (4)$$

where $\kappa_{c(m)} = [\kappa_{c(m),L} + \kappa_{c(m),R}]/2$. We introduce η and δ as two phenomenological parameters to account for the anomalous period and coupling rate, respectively.

Using Eq. (4), the transmission $S_{21} = \hat{s}_{-2}/\hat{s}_{+1}$ of coupled system is derived as

$$S_{21} = \frac{[\omega - \tilde{\omega}_m + i(1 - \delta^2)\kappa_{m,R}](\omega - \tilde{\omega}_c) - G_0^2}{(\omega - \tilde{\omega}_m + i\kappa_{m,R})(\omega - \tilde{\omega}_c + i\kappa_{c,R}) + Ke^{i2\Phi/\eta}}, \quad (5)$$

where $G_0^2 = -\kappa_{c,R}\kappa_{m,R}(1-\delta)[e^{i2\Phi/\eta}\sqrt{(\kappa_{c,L}\kappa_{m,L}/\kappa_{c,R}\kappa_{m,R})}-\delta]$ and $K = \sqrt{\kappa_{c,R}\kappa_{m,R}\kappa_{c,L}\kappa_{m,L}}$.

Setting $\eta = 1$ and $\delta = 1$, Eqs. (4) and (5) reproduce the standard theory describing photon-mediated coupling [19]. Using the parameters calibrated in Table I for $d = 6.90$ mm and setting $\Phi = (2n+1)\pi$ with n as an integer [35], the calculated $|S_{21}(\omega)|$ spectra plotted by the dotted curves in Fig. 4(d) qualitatively agree with the measured spectra. Furthermore, as shown by the dotted curve plotted in Fig. 3(f), the Φ dependence of $1/|S_{21}(\omega_c)|$ calculated for $\Phi \in [2n\pi, 2(n+1)\pi]$ qualitatively agrees with the measured data [62], showing that the observed oscillation originates from the photon-mediated coupling term $Ke^{i2\Phi}$ in Eq. (5). Smoking guns of deviation from the standard theory are evident, but hard to verify from the experiments performed at such noncritical coupling settings.

In contrast, at $d = 4.92$ mm, $|S_{21}(\omega)|$ calculated from the standard theory ($\eta = 1$ and $\delta = 1$) fails completely to reproduce the observed splitting at $\Delta_m = 0$, as shown by the black dotted curve plotted in Fig. 4(b). Moreover, it fails to explain the observed amplitude of the magnonlike mode measured at $\Delta_m \neq 0$. Here, we have to set $\delta = 0.996$ to reproduce the observed mode splitting at $\Delta_m = 0$, as shown by the red dashed curve plotted in Fig. 4(b). Furthermore, we need to set $\eta = 2$ to account for the anomalous phase period, as shown by the red dashed curves plotted in Figs. 3(a) and 3(b). Setting $\eta = 2$ also reproduces the amplitude of the magnonlike mode, as shown by the dashed curves plotted in Fig. 4(b). Thus, critically driven cavity magnonics reveals two anomalous features in contrast to conventional cases [19–22]: (i) the photon-mediated coherence is no longer exactly erased by the photon-induced decoherence, and (ii) the phase period of the coupling strength is doubled.

Currently, there is no theory suitable for explaining these anomalies. To examine whether our discovery is limited to special cavities with specific geometric parameters, we replace the 3D cylindrical cavity with a 2D complementary split-ring resonator. Near the critically driven condition, the experimental results [35] well reproduce both anomalies, indicating that the phase-dependent anomalous coupling may be universal and deserves deep investigation.

Conclusion.—By coupling a YIG sphere remotely through cables over 2 m long with either a cylindrical cavity or a ring resonator, we discover an anomalous long-distance strong coupling. Our experiments show that critically driven cavity functions as a loaded high-Q oscillator with nearly zero damping, which is extremely sensitive to detect long-distance coupling. Phase-dependent measurements show unambiguously that the observed remote coupling is mediated by the traveling photons, and the field-dependent measurements directly demonstrate coherent energy exchange between a pair of local oscillators separated by a macroscopic distance. We find that the coupling strength oscillates exactly twice the period of conventional photon-mediated couplings. Both anomalies are found independent of specific geometric parameters of the cavity, demonstrating that critically driven cavity magnonics is a robust platform for harnessing long-distance coherence, which may open new horizons for developing cavity magnonics networks. The observed anomalies may generate broad interest for theoretical and experimental studies of photon-mediated coherence and remote sensing in coupled system of distributed oscillators.

*Corresponding author: hu@physics.umanitoba.ca; http://www.physics.umanitoba.ca/~hu

[1] D. E. Chang, J. S. Douglas, A. González-Tudela, C.-L. Hung, and H. J. Kimble, Colloquium: Quantum matter built from nanoscopic lattices of atoms and photons, Rev. Mod. Phys. **90**, 031002 (2018).

[2] B. Z. Rameshti, S. V. Kusminskiy, J. A. Haigh, K. Usami, D. Lachance-Quirion, Y. Nakamura, C.-M. Hu, H. X. Tang, G. E. Bauer, and Y. M. Blanter, Cavity magnonics, Phys. Rep. **979**, 1 (2022).

[3] A. V. Chumak, P. Kabos, M. Wu, C. Abert, C. Adelmann, A. O. Adeyeye, J. Åkerman, F. G. Aliev, A. Anane, A. Awad *et al.*, Advances in magnetics roadmap on spin-wave computing, IEEE Trans. Mag. **58**, 1 (2022).

[4] A. Xuereb, C. Genes, and A. Dantan, Strong coupling and long-range collective interactions in optomechanical arrays, Phys. Rev. Lett. **109**, 223601 (2012).

[5] Y. Li, V. G. Yefremenko, M. Lisovenko, C. Trevillian, T. Polakovic, T. W. Cecil, P. S. Barry, J. Pearson, R. Divan, V. Tyberkevych *et al.*, Coherent coupling of two remote magnonic resonators mediated by superconducting circuits, Phys. Rev. Lett. **128**, 047701 (2022).

[6] B. Hetényi, A. Mook, J. Klinovaja, and D. Loss, Long-distance coupling of spin qubits via topological magnons, Phys. Rev. B **106**, 235409 (2022).

[7] M. J. A. Schuetz, E. M. Kessler, G. Giedke, L. M. K. Vandersypen, M. D. Lukin, and J. I. Cirac, Universal quantum transducers based on surface acoustic waves, Phys. Rev. X **5**, 031031 (2015).

[8] M. F. Yanik and S. Fan, Time reversal of light with linear optics and modulators, Phys. Rev. Lett. **93**, 173903 (2004).

[9] Q. Xu, S. Sandhu, M. L. Povinelli, J. Shakya, S. Fan, and M. Lipson, Experimental realization of an on-chip all-optical analogue to electromagnetically induced transparency, Phys. Rev. Lett. **96**, 123901 (2006).

[10] D.-W. Luo, X.-F. Qian, and T. Yu, Nonlocal magnon entanglement generation in coupled hybrid cavity systems, Opt. Lett. **46**, 1073 (2021).

[11] D. Mukhopadhyay, J. M. P. Nair, and G. S. Agarwal, Anti-pt symmetry enhanced interconversion between microwave and optical fields, Phys. Rev. B **105**, 064405 (2022).

[12] A. Metelmann and A. A. Clerk, Nonreciprocal photon transmission and amplification via reservoir engineering, Phys. Rev. X **5**, 021025 (2015).

[13] Y.-P. Wang, J. W. Rao, Y. Yang, P.-C. Xu, Y. S. Gui, B. M. Yao, J. Q. You, and C.-M. Hu, Nonreciprocity and unidirectional invisibility in cavity magnonics, Phys. Rev. Lett. **123**, 127202 (2019).

[14] P. Lodahl, S. Mahmoodian, S. Stobbe, A. Rauschenbeutel, P. Schneeweiss, J. Volz, H. Pichler, and P. Zoller, Chiral quantum optics, Nature (London) **541**, 473 (2017).

[15] A. P. Foster, D. Hallett, I. V. Iorsh, S. J. Sheldon, M. R. Godsland, B. Royall, E. Clarke, I. A. Shelykh, A. M. Fox, M. S. Skolnick, I. E. Itskevich, and L. R. Wilson, Tunable photon statistics exploiting the fano effect in a waveguide, Phys. Rev. Lett. **122**, 173603 (2019).

[16] A. S. Sheremet, M. I. Petrov, I. V. Iorsh, A. V. Poshakinskiy, and A. N. Poddubny, Waveguide quantum electrodynamics: collective radiance and photon-photon correlations, Rev. Mod. Phys. **95**, 015002 (2023).

[17] M. Mirhosseini, E. Kim, X. Zhang, A. Sipahigil, P. B. Dieterle, A. J. Keller, A. Asenjo-Garcia, D. E. Chang, and O. Painter, Cavity quantum electrodynamics with atom-like mirrors, Nature (London) **569**, 692 (2019).

[18] N. V. Corzo, J. Raskop, A. Chandra, A. S. Sheremet, B. Gouraud, and J. Laurat, Waveguide-coupled single collective excitation of atomic arrays, Nature (London) **566**, 359 (2019).

[19] S. Fan, W. Suh, and J. D. Joannopoulos, Temporal coupled-mode theory for the fano resonance in optical resonators, J. Opt. Soc. Am. A **20**, 569 (2003).

[20] K. Lalumiere, B. C. Sanders, A. F. van Loo, A. Fedorov, A. Wallraff, and A. Blais, Input-output theory for waveguide QED with an ensemble of inhomogeneous atoms, Phys. Rev. A **88**, 043806 (2013).

[21] L. F. Buchmann and D. M. Stamper-Kurn, The quantum/classical transition in mediated interactions, Ann. Phys. (Berlin) **527**, 156 (2015).

[22] T. M. Karg, B. Gouraud, P. Treutlein, and K. Hammerer, Remote Hamiltonian interactions mediated by light, Phys. Rev. A **99**, 063829 (2019).

[23] J. Majer, J. Chow, J. Gambetta, J. Koch, B. Johnson, J. Schreier, L. Frunzio, D. Schuster, A. A. Houck, A. Wallraff *et al.*, Coupling superconducting qubits via a cavity bus, Nature (London) **449**, 443 (2007).

[24] P. Y. Wen, K.-T. Lin, A. F. Kockum, B. Suri, H. Ian, J. C. Chen, S. Y. Mao, C. C. Chiu, P. Delsing, F. Nori, G. D. Lin, and I. C. Hoi, Large collective lamb shift of two distant superconducting artificial atoms, Phys. Rev. Lett. **123**, 233602 (2019).

[25] K.-T. Lin, T. Hsu, C.-Y. Lee, I.-C. Hoi, and G.-D. Lin, Scalable collective lamb shift of a 1d superconducting qubit array in front of a mirror, Sci. Rep. **9**, 19175 (2019).

[26] T. M. Karg, B. Gouraud, C. T. Ngai, G.-L. Schmid, K. Hammerer, and P. Treutlein, Light-mediated strong coupling between a mechanical oscillator and atomic spins 1 meter apart, Science **369**, 174 (2020).

[27] A. F. Kockum, G. Johansson, and F. Nori, Decoherence-free interaction between giant atoms in waveguide quantum electrodynamics, Phys. Rev. Lett. **120**, 140404 (2018).

[28] B. Kannan, M. J. Ruckriegel, D. L. Campbell, A. Frisk Kockum, J. Braumüller, D. K. Kim, M. Kjaergaard, P. Krantz, A. Melville, B. M. Niedzielski *et al.*, Waveguide quantum electrodynamics with superconducting artificial giant atoms, Nature (London) **583**, 775 (2020).

[29] Z.-Q. Wang, Y.-P. Wang, J. Yao, R.-C. Shen, W.-J. Wu, J. Qian, J. Li, S.-Y. Zhu, and J. You, Giant spin ensembles in waveguide magnonics, Nat. Commun. **13**, 7580 (2022).

[30] B. Yao, Y. S. Gui, J. W. Rao, Y. H. Zhang, W. Lu, and C.-M. Hu, Coherent microwave emission of gain-driven polaritons, Phys. Rev. Lett. **130**, 146702 (2023).

[31] J. W. Rao, C. Y. Wang, B. M. Yao, Z. J. Chen, K. X. Zhao, and W. Lu, Meterscale strong coupling between magnons and photons, Phys. Rev. Lett. **131**, 106702 (2023).

[32] Y. Yang, Y.-P. Wang, J. W. Rao, Y. S. Gui, B. M. Yao, W. Lu, and C.-M. Hu, Unconventional singularity in anti-parity-time symmetric cavity magnonics, Phys. Rev. Lett. **125**, 147202 (2020).

[33] A. Petosa, *Dielectric Resonator Antenna Handbook* (Artech, London, 2007).

[34] A. Serga, A. Chumak, and B. Hillebrands, Yig magnonics, J. Phys. D **43**, 264002 (2010).

[35] See Supplemental Material at http://link.aps.org/supplemental/10.1103/PhysRevLett.132.206902 for detailed description of theoretical and experimental methods, which includes Refs. [36–51].

[36] C. Manolatou, M. J. Khan, S. Fan, P. R. Villeneuve, H. A. Haus, and J. D. Joannopoulos, Coupling of modes analysis of resonant channel add-drop filters, IEEE J. Quantum Electron. **35**, 1322 (1999).

[37] W. Suh, Z. Wang, and S. Fan, Temporal coupled-mode theory and the presence of non-orthogonal modes in lossless multimode cavities, IEEE J. Quantum Electron. **40**, 1511 (2004).

[38] Z. Zhao, C. Guo, and S. Fan, Connection of temporal coupled-mode-theory formalisms for a resonant optical system and its time-reversal conjugate, Phys. Rev. A **99**, 033839 (2019).

[39] A. Yariv, Universal relations for coupling of optical power between microresonators and dielectric waveguides, Electron. Lett. **36**, 321 (2000).

[40] M. Cai, O. Painter, and K. J. Vahala, Observation of critical coupling in a fiber taper to a silica-microsphere whispering-gallery mode system, Phys. Rev. Lett. **85**, 74 (2000).

[41] S. Darmawan, Y. M. Landobasa, and M. K. Chin, Phase engineering for ring enhanced Mach-Zehnder interferometers, Opt. Express **13**, 4580 (2005).

[42] I. Demirtzioglou, C. Lacava, K. R. Bottrill, D. J. Thomson, G. T. Reed, D. J. Richardson, and P. Petropoulos, Frequency comb generation in a silicon ring resonator modulator, Opt. Express **26**, 790 (2018).

[43] Y. Ra'di, A. Krasnok, and A. Alú, Virtual critical coupling, ACS Photonics **7**, 1468 (2020).

[44] F. Monifi, J. Friedlein, Ş. K. Özdemir, and L. Yang, A robust and tunable add–drop filter using whispering gallery mode microtoroid resonator, J. Lightwave Technol. **30,** 3306 (2012).

[45] J. Yoon, K. H. Seol, S. H. Song, and R. Magnusson, Critical coupling in dissipative surface-plasmon resonators with multiple ports, Opt. Express **18,** 25702 (2010).

[46] S. Wan, R. Niu, H.-L. Ren, C.-L. Zou, G.-C. Guo, and C.-H. Dong, Experimental demonstration of dissipative sensing in a self-interference microring resonator, Photonics Res. **6,** 681 (2018).

[47] W. Liu, Y. Lin, J. Li, and X. Wang, Nonreciprocal waveguide-QED for spinning cavities with multiple coupling points, Front. Phys. **10,** 894115 (2022).

[48] A. F. Kockum, P. Delsing, and G. Johansson, Designing frequency-dependent relaxation rates and lamb shifts for a giant artificial atom, Phys. Rev. A **90,** 013837 (2014).

[49] S. Zanotto, F. P. Mezzapesa, F. Bianco, G. Biasiol, L. Baldacci, M. S. Vitiello, L. Sorba, R. Colombelli, and A. Tredicucci, Perfect energy-feeding into strongly coupled systems and interferometric control of polariton absorption, Nat. Phys. **10,** 830 (2014).

[50] D. Zhang, X.-Q. Luo, Y.-P. Wang, T.-F. Li, and J. You, Observation of the exceptional point in cavity magnon-polaritons, Nat. Commun. **8,** 1368 (2017).

[51] M. Harder, L. H. Bai, C. Match, J. Sirker, and C.-M. Hu, Study of the cavity-magnon-polariton transmission line shape, Sci. China Phys. Mech. Astron. **59,** 117511 (2016).

[52] D. M. Pozar, *Microwave Engineering* (John wiley & sons, New York, 2011).

[53] C. W. Gardiner and M. J. Collett, Input and output in damped quantum systems: Quantum stochastic differential equations and the master equation, Phys. Rev. A **31,** 3761 (1985).

[54] T. Yu, X. Zhang, S. Sharma, Y. M. Blanter, and G. E. W. Bauer, Chiral coupling of magnons in waveguides, Phys. Rev. B **101,** 094414 (2020).

[55] F. Bo, Ş. K. Özdemir, F. Monifi, J. Zhang, G. Zhang, J. Xu, and L. Yang, Controllable oscillatory lateral coupling in a waveguide-microdisk-resonator system, Sci. Rep. **7,** 8045 (2017).

[56] Y.-T. Chen, L. Du, L. Guo, Z. Wang, Y. Zhang, Y. Li, and J.-H. Wu, Nonreciprocal and chiral single-photon scattering for giant atoms, Commun. Phys. **5,** 215 (2022).

[57] H. Haus, W. Huang, S. Kawakami, and N. Whitaker, Coupled-mode theory of optical waveguides, J. Lightwave Technol. **5,** 16 (1987).

[58] W.-P. Huang, Coupled-mode theory for optical waveguides: An overview, J. Opt. Soc. Am. A **11,** 963 (1994).

[59] M. Ghulinyan, F. Ramiro-Manzano, N. Prtljaga, R. Guider, I. Carusotto, A. Pitanti, G. Pucker, and L. Pavesi, Oscillatory vertical coupling between a whispering-gallery resonator and a bus waveguide, Phys. Rev. Lett. **110,** 163901 (2013).

[60] A. F. Van Loo, A. Fedorov, K. Lalumiere, B. C. Sanders, A. Blais, and A. Wallraff, Photon-mediated interactions between distant artificial atoms, Science **342,** 1494 (2013).

[61] A. Tiranov, V. Angelopoulou, C. J. van Diepen, B. Schrinski, O. A. D. Sandberg, Y. Wang, L. Midolo, S. Scholz, A. D. Wieck, A. Ludwig *et al.*, Collective super- and subradiant dynamics between distant optical quantum emitters, Science **379,** 389 (2023).

[62] The parameters $\kappa_{c,L(R)}$ change slightly by changing Φ, which we have calibrated in [35].